Journal of Arid Environments 112 (2015) 75–86

Contents lists available at ScienceDirect

Journal of Arid Environments

journal homepage: www.elsevier.com/locate/jaridenv

Identification and characterization of Biological Soil Crusts in a sand dune desert environment across Israel–Egypt border using LWIR emittance spectroscopy

Offer Rozenstein, Arnon Karnieli*

The Remote Sensing Laboratory, Jacob Blaustein Institutes for Desert Research, Ben-Gurion University of the Negev, Sede Boqer Campus 84990, Israel

ARTICLE INFO

Article history:
Received 4 July 2013
Received in revised form
25 November 2013
Accepted 27 January 2014
Available online 28 February 2014

Keywords:
Biological Soil Crusts
Emittance spectroscopy
LWIR
Thermal remote sensing

ABSTRACT

Biological Soil Crusts (BSCs) are critical components of desert ecosystems worldwide. While all BSCs significantly modify the surfaces they occupy, the manner in which they affect their environment depends on the composition of the microphytic community. The aim of this paper is to study the hyperspectral thermal emissivity signatures of BSCs in order to identify and characterize them in a sand dune environment. The research was conducted in the northwestern Negev dunes. Measurements of several types of BSCs and bare soil were obtained using ground hyperspectral thermal sensors. We present an ability to spectrally separate different types of BSCs from bare sand, and to rank them according to successional development. Based on this ability, we created a spectral index for the discrimination of sand and BSCs of different types and applied it to multispectral remote sensing thermal images. This newly acquired ability to map different BSC types, using remote sensing, may lead to future applications of habitat and ecological function spatial mapping. We also demonstrate how a fusion of reflective and thermal data can be used to map different land-cover features in a sand dune environment. Our proposed thermal index not only discriminates sand and BSCs, but also enhances the signal from limestone pebbles more than other indices, based on reflective data. Unlike remote sensing in the reflective spectral region, thermal remote sensing is unconstrained by solar illumination. High resolution emissivity signatures of land cover are unaffected by environmental variables, as opposed to land-surface temperature that depends on the time of day and the season.

1. Introduction

Biological Soil Crusts (BSCs) cover vast regions in drylands worldwide. BSCs consist of soil granules and various microphytic communities, including cyanobacteria, algae, mosses, lichens, and fungi (West, 1990). BSCs are important components in dryland ecosystems. They are involved in soil stabilization and the prevention of wind and water erosion (Bowker, 2007), carbon and nitrogen fixation (Burgheimer et al., 2006; Wu et al., 2009), and hydrological processes (Belnap, 2006), and they have complex interactions with flora (Boeken et al., 2004; Serpe et al., 2006) and fauna (Bamforth, 2008). While BSCs perform vital ecosystem functions, differences in species composition and abundance affect the rate and nature of these functions. Many examples for this can be found in the literature: for instance, an increase in numbers/biomass of cyanobacteria increases soil stability (Belnap et al., 2008). In the absence of mosses and lichens, newly developed cyanobacterial BSC is very thin and fragile, and thus folds off the ground when desiccation is rapid (Zaady, 1999). The fixation rates of carbon and nitrogen are higher in later successional BSCs than in the earlier successional BSCs (Housman et al., 2006). Nematode communities were found to be successionally more mature beneath well-developed, late-successional stage crusts than beneath immature, early-successional stage crusts (Darby et al., 2007). Lizards prefer to dig their burrows in fragile, rather than in hard, BSC (Zaady and Bouskila, 2002). The mechanical resistance to disturbance by trampling is higher in cyanobacteria than in lichens, and lichens are more resistant than mosses (Belnap and Eldridge, 2001; Jimenez Aguilar et al., 2009). These examples demonstrate that in order to understand the condition of a site, it is important to assess the level of development of BSCs, not just their cover. As knowledge on the ecological functions of BSCs continues to accumulate, it becomes clearer that the BSCs' successional level of development critically influences these functions.

* Corresponding author. Tel.: +972 8 659 6855, +972 52 879 5925 (mobile); fax: +972 8 6596805.
E-mail addresses: oferroz@bgu.ac.il (O. Rozenstein), karnieli@bgu.ac.il (A. Karnieli).

http://dx.doi.org/10.1016/j.jaridenv.2014.01.017

An assortment of destructive analysis techniques has been developed for determining the BSCs' level of development. These methods include field and laboratory testing, such as measuring crust thickness using a vernier caliper, and measuring hardness using a soil penetrometer to evaluate resistance to compressive force (Guo et al., 2008). These methods assume that the thickness and hardness of BSCs increase with BSC development. Other laboratory methods are able to infer the BSCs' successional stage based on a phospholipid fatty acid, or denaturing gradient gel electrophoresis (Ben-David et al., 2011; Zaady et al., 2010), the phytomass of algae and lichens (West, 1990) or by quantifying chlorophyll, polysaccharide, and protein content (Zaady and Bouskila, 2002). While these techniques are all valid and accepted ways of estimating BSCs' level of development, they all require disturbances of the soil surface by removing the crust for laboratory analyses.

One way to analyze BSCs without disturbing them is by using spectroscopy (Zaady et al., 2007). Another advantage of spectroscopy is the ability to up-scale the ground spectral measurements of field samples to analyze remote sensing data and to create spatial maps (Milton et al., 2009; Schaepman et al., 2009). This ability to extend site-specific ecological studies to a regional scale reduces the time and cost associated with ground surveys. Previous studies have demonstrated that BSCs possess unique spectral-phenological characteristics in the visible, near-infrared and short-wave infrared (VIS-NIR-SWIR; 0.4–2.5 mm) (Karnieli et al., 2001, 2002). This enables the use of spectroscopy and remote sensing to map their distribution in relation to microphytic vegetation and bare soil (Karnieli, 2003). Several indices were used to identify cyanobacteria-dominated BSCs (Karnieli, 1997; Moghtaderi et al., 2011) and lichen-dominated BSCs (Chen et al., 2005), using multispectral remote sensing. Other studies used hyperspectral imagery for mapping BSCs. These studies only identified BSCs as distinguished from other land-cover types (Weber et al., 2008) or classified different treatments, such as irrigation and disturbance (Ustin et al., 2009). While these previous studies employed reflectance spectroscopy to this end, thermal infrared (TIR) data has rarely been used to study BSCs.

Remote sensing of BSCs in the TIR has been previously accomplished using just one or two wide spectral bands in the long-wave infrared (LWIR) spectral region (8–12 μm). These studies have shown differences in land surface temperature between crusted sand dunes and bare sand (Qin et al., 2001, 2002), and demonstrated that this phenomenon occurs since BSCs have a higher emissivity than bare sand (Qin et al., 2005). These emissivity measurements were performed using just one wide band covering 8–14 μm. Therefore, to the best of our knowledge, the emissivity spectra of BSCs have not been measured using high spectral resolution.

In recent years, LWIR remote sensing development has followed a progression toward higher spectral resolution in the drive toward identifying materials based on their emissive spectra (Collins, 1996). The Thermal Infrared Multispectral Scanner (TIMS) (Kahle and Goetz, 1983) and, later, the hyperspectral Spatially Enhanced Broadband Array Spectrograph System (SEBASS) have been successfully used to map a variety of rocks and minerals (Kirkland et al., 2002; Vaughan et al., 2003, 2005). Field and laboratory LWIR spectra of vegetation produced useful information about leaf chemistry and structure. In contrast with VIS-NIR-SWIR data, TIR spectral information is more species specific, and the applications, therefore, are different (Ribeiro da Luz and Crowley, 2007). SEBASS is the first instrument to achieve the necessary data quality for discerning TIR spectral features in plants, and to identify a variety of plant species (Ribeiro da Luz and Crowley, 2010). However, the mapping of BSCs' successional level may prove to be easier than that of higher vegetation species, because of less volume scattering

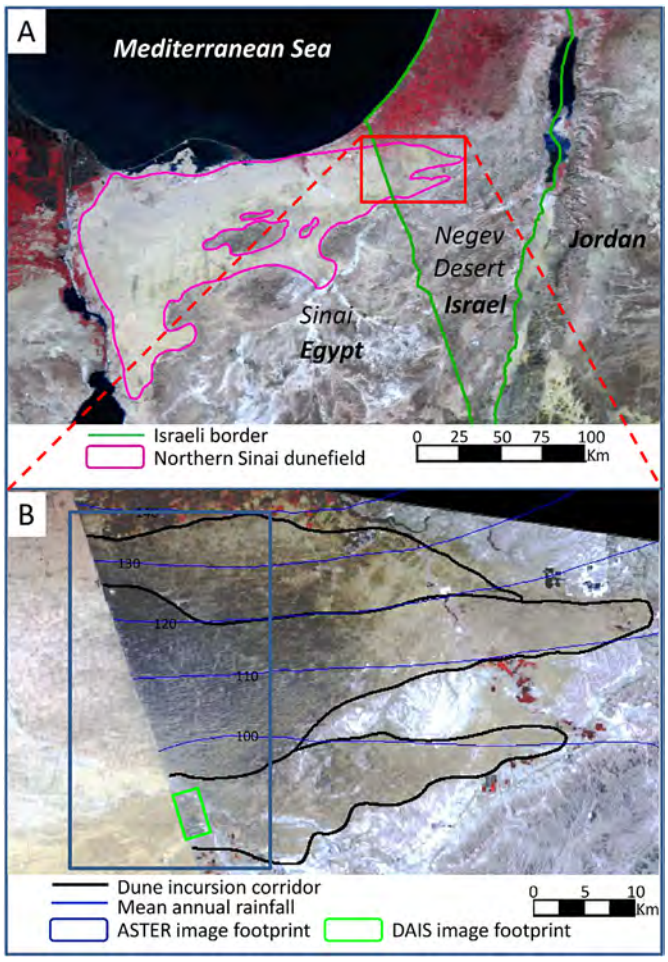

Fig. 1. (A) MODID false color regional image (RGB = 2,1,4) of the research site acquired on Feb. 4, 2012. The Northern Sinai dune field is shown to cross the Israeli–Egyptian political border into the northwestern Negev. The red rectangle represents the footprint of Fig. 1B; (B) Landsat-5 false color image (RGB = 4,3,2) of the research site (path 174, row 39) acquired on Jun. 14, 2000. The thick lines mark the dune incursion corridor classification (Roskin et al., 2011b). The isohyets represent the mean annual rainfall for 1986–2006 (Siegal et al., 2013). The green rectangle represents the footprint of the images displayed in Figs. 5–7. The Israel–Egypt border line is evident from the sharp brightness contrast between the Negev and Sinai. This contrast is the result of different land-use management: the prevention of anthropogenic pressures has allowed Biological Soil Crusts (BSCs) to establish and stabilize the dunes in the Negev, while grazing and trampling in Sinai prevent BSC establishment and maintain the dunes in a mobile state, and covered mostly by bright bare sands. (For interpretation of the references to color in this figure legend, the reader is referred to the web version of this article.)

than in tree canopies that constrains species identification (Ribeiro da Luz and Crowley, 2007; Ribeiro da Luz and Crowley, 2010) and less volume scattering than in powder minerals (Salisbury and Wald, 1992). This means that BSCs' LWIR spectra are expected to be less noisy for the same species. One study has shown that lichens' spectra have a remarkably uniform curved shape that appears related to lichen texture (Salisbury and D'Aria, 1992). LWIR spectroscopy and remote sensing possess several advantages over the traditional reflective part of the spectrum. This technology is unconstrained by solar illumination, thus enabling data collection at night, or under cloud and smoke cover. In addition, the LWIR spectral region is better suited for the exploration of certain materials. For example, quartz does not provide any usable feature in the VIS-NIR-SWIR wavelength region. However, in the LWIR, quartz displays a broad emissivity doublet between 8 and 10 μm (Eisele

et al., 2012). Therefore, it seems that multispectral and hyperspectral LWIR remote sensing is suitable for measurements of BSCs on a quartz-based substrate.

Hence, the primary aim of this paper is to explore the spectroscopic features of BSC in the LWIR in a desert dune environment. Specific objectives are:

1. To characterize the spectral signatures of different Biological Soil Crusts using emission spectroscopy in the TIR region, with respect to dune sand.
2. To develop a spectral crust index based on LWIR data and compare its performance to the original crust index based on reflective data (Karnieli, 1997).
3. To demonstrate the advantage of using high spectral resolution LWIR remote sensing over mono/dual band methods.
4. To explore the potential for data fusion of reflective and TIR data for land-cover mapping.

2. Material and methods

2.1. Study area

The northwestern Negev dunes are a part of the northern Sinai erg, split only by the political Israel–Egypt border (Fig. 1) (Roskin et al., 2011a). Due to the geopolitical circumstances, access to the Egyptian side is restricted, making remote sensing a valuable research tool. While the linear dunes are transected by the border, there are no differences in geology or climate between its two sides. The only difference is the land-use policy implemented by both countries: after the border was last closed in 1982, human-induced activity on the Israeli side has subsided, while on the Egyptian side, Bedouin pastoralists continue grazing and wood gathering activities (Karnieli and Tsoar, 1995; Tsoar et al., 2008). Grazing by sheep, goats, and camels in Sinai, and, in particular, the trampling on the dune surface have inhibited the establishment of BSCs. Therefore, the dunes in Sinai are active shifting sands. On the Israeli side of the border, the sparse anthropogenic activity has allowed BSCs to establish themselves on the dunes, fixing them, leaving only a small active portion on the dune crest. Since most of the surface on the Negev side is composed of BSCs, and most of the surface on the Sinai side is covered by sand (Qin et al., 2006), a brightness contrast is visible in satellite images of reflective spectral data (Tsoar and Karnieli, 1996). This contrast in land cover has also created a thermal anomaly; since the emissivity of BSCs is higher than that of sand, the Negev dune field can be as much as 4 °C warmer than the Sinai side of the border (Karnieli and Dall'Olmo, 2003). However, at night as the temperature equalizes on both sides of the border, this temperature contrast disappears (Qin et al., 2002).

The study area is characterized by mean monthly temperatures ranging from 9 °C in January to 27 °C in August, and a sharp rainfall gradient from below 100 mm in the south to above 140 mm in the north, over a distance of 30 km (Siegal et al., 2013). Dune morphology is not consistent over the entire region as three incursion corridors, each characterized by different morphologies, can be classified (Roskin et al., 2011b): the northern corridor is characterized by low, vegetated linear dunes with wide interdune areas; the central corridor is characterized by high, vegetated linear dunes with some crescentic dunes connecting them in the interdune areas; the southern corridor is characterized by high, vegetated linear dunes, composed of sand that is more reddish than the sand in the former unit and without any crescentic dunes in the interdune area. Fig. 1B displays the precipitation gradient along with the dune incursion corridors. Past dune encroachment from the Northern Sinai Peninsula into the northwestern Negev dammed

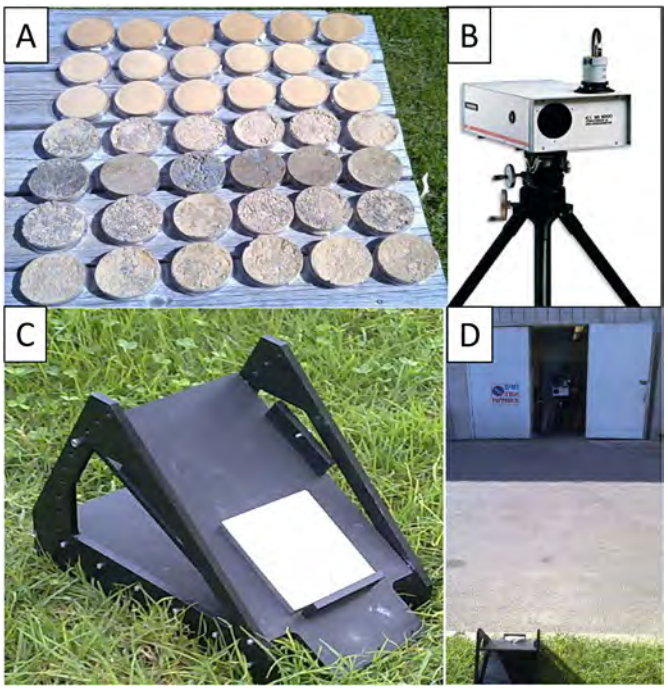

Fig. 2. (A) Sand and Biological Soil Crusts samples laid out in the sun to warm up. Warming up the samples prior to measurement increases the target signal; (B) The SR-5000 spectroradiometer; (C) An apparatus used to tilt the samples towards the spectroradiometer. The tilt angle must be lower than 33° in order to keep the sand from spilling over. A silver-coated mirror used to measure the sky irradiance is placed on top of the tilted surface; (D) The SR-5000 operated from a hanger and pointed towards a target sample.

wadis and formed unique shallow standing water bodies in the southern and eastern dunefield fringe (Magaritz and Enzel, 1990). The ponded water extended upstream and into interdune spaces, depositing whitish-gray paludal sediments that are easily discerned in the field and from the air by their brightness and flat appearance. These areas will be referred to as "playas". Since the development of BSCs is affected by moisture availability, BSCs in the north are more developed than those in the south. The dunes' topography and orientation create a micro-meteorological effect on the development of BSCs, such that the BSCs on the northern slopes are more developed than those on the southern slopes and interdune areas. BSCs' species classification has been described elsewhere in the literature (Büdel and Veste, 2008; e.g. Karnieli et al., 1999; Veste et al., 2001). More recent studies have found differences in vegetation cover between the two sides of the border with about 16% vegetation cover in the Negev and 6% in Sinai (Qin et al., 2006; Seifan, 2009). In the Negev's northern and central incursion corridors, vegetation cover is about 10–20% while in the southern corridor, only 5–13% (Siegal et al., 2013).

2.2. Ground spectral measurements

50 BSCs and sand samples were collected from the Negev sand dunes. BSCs were collected from northern slopes, southern slopes, and interdune areas, while sand was collected from dune crests. Note that the latter samples also represent the Sinai sands. Samples were collected from the southern and central incursion corridors. Physical crust from the playas in the southern incursion corridor was also collected. The SR-5000 spectroradiometer was used to measure the samples (Cabib et al., 2004). The measurement took place outdoors on a warm summer day, with a clear sky. Prior to measurement, the dry samples were placed in the sun to warm up.

This was intended to increase the signal emitted by the samples, and also to bring the samples to thermal equilibrium and reduce any thermal gradients with the environment. Since the SR-5000 cannot be tilted to view the ground at nadir, it was only tilted down at about 15°. In order to tilt the samples toward the spectroradiometer aperture, without spilling the sand, we placed them on a sloped surface with a tilt of approximately 25° relative to the floor (Fig. 2). The spectroradiometer was calibrated against a blackbody target at 45 °C and an internal blackbody at ambient temperature to produce the measured signal in radiance units. The spectral radiance for each sample ($L_{meas}(\lambda)$) was produced by averaging 30 readings. In order to convert the samples' radiance into emissivity, the sample temperature was estimated by fitting Planck blackbody radiance curves ($L_{BB}(\lambda,T)$) to the samples' radiance curves while iterating the blackbody temperature (T) until the target radiance curve was just under the blackbody radiance curve:

$$L_{BB}(\lambda,T) = 2hc^2/\lambda^5\left(e^{\frac{kc}{\lambda kT}}-1\right) \quad (1)$$

where: h is the Plank's constant ($6.626\cdot10^{-34}$ J·s), c is the speed of light (2.99 msec^{-2}), and K is the Boltzmann constant ($1.38\cdot10^{-23}$ J).

The temperature estimates were compared to kinetic temperature measurements by a thermocouple taken just before each reading, and were found to be accurate to about 1 °C. The downwelling sky radiance ($L_{DW}(\lambda)$) was derived by measuring a silver-coated mirror. Thus, sample emissivity ($\varepsilon_T(\lambda)$) was calculated according to Horton et al. (1998):

$$\varepsilon_T(\lambda) = \frac{L_{meas}(\lambda)-L_{DW}(\lambda)}{L_{BB}(\lambda)-L_{DW}(\lambda)} \quad (2)$$

The spectral radiance of the atmospheric path between the target and the instrument was neglected since the path distance was relatively short (<10 m).

Based on the samples' emissivity spectra, an index was created to differentiate between the sand and BSCs at different successional levels. This index will be referred to hereafter as the Thermal Crust Index (TCI). Although the derivation of the TCI was based on hyperspectral signatures, we only used two bands to formalize the index since the remote sensing images available to us were multispectral (discussed in the next two sections).

2.3. Spaceborne images

The Advanced Spaceborne Thermal Emission and Reflection Radiometer (ASTER) sensor is an imaging instrument flown on the Terra satellite that was launched in December 1999. ASTER is a cooperative effort between NASA and Japan and has been designed to acquire land surface temperature, emissivity, reflectance, and elevation data (Kahle et al., 1991). ASTER has multispectral TIR capabilities, with five bands in the LWIR region, at a spatial resolution of 90 m. Relatively cloud-free ASTER images over the research area, from both day and night, are available. We used a Level-2B AST_05 Surface Emissivity product. This product is produced from the five atmospherically corrected LWIR ASTER bands through the Temperature-Emissivity Separation (TES) algorithm (Gillespie et al., 1998). Since the spatial resolution of the product is only 90 m, mixing of different land covers (i.e., bare sand, vegetation, BSCs of different successional stages, etc.) occurs within each pixel. For this reason, no pure spectral signatures can be extracted from the image, making it difficult to directly compare observations of each distinct land-cover type. However, due to the fact that the majority of land cover on the Israeli side is BSCs, and the majority of land cover on the Egyptian side is bare sand, it was possible to make a comparison between the two sides of the border. To account for differences in BSC development, we sampled three pairs of polygons along the rain gradient, one pair in each of the dune incursion corridors. In addition, we examined both day and night surface emissivity products, and applied to them the newly formalized TCI. Even though it is doubtful that the sparse vascular vegetation will change the pixel signature very much, its effect on the emissivity observed from space was minimized by using images from the end of summer. In this season, the vegetation cover is minimal since perennial plants are dominant, the annual vegetation has dried up, and much of the plant litter has been blown away by the wind.

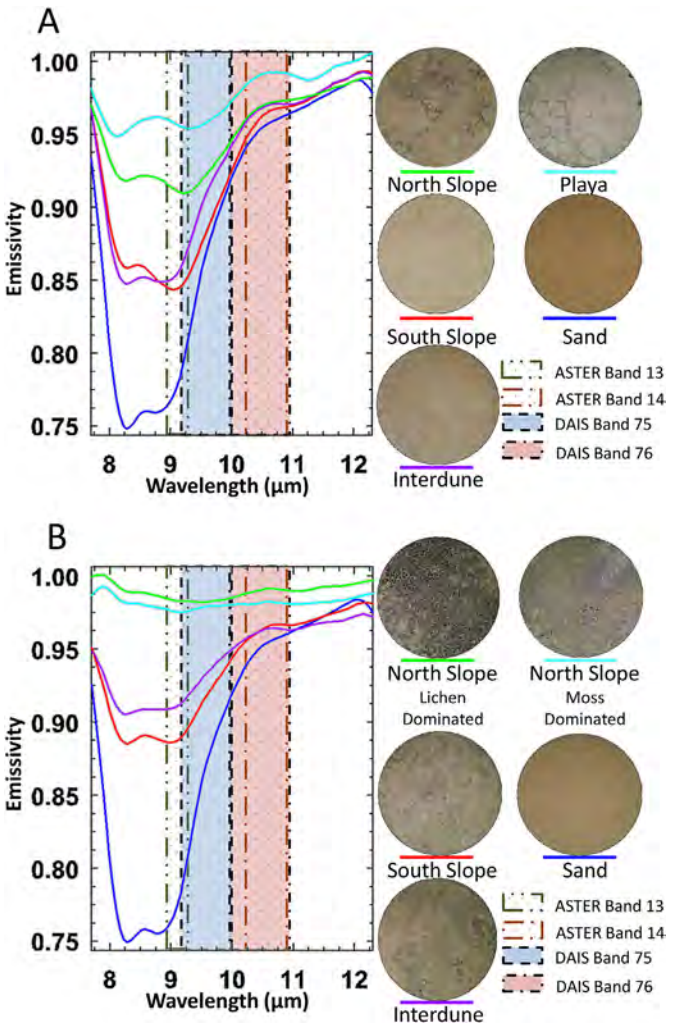

Fig. 3. LWIR spectral signatures of sand and soil crusts from (A) the southern dune incursion corridor imposed on top are the ASTER and DAIS bands used in the formulation of the Thermal Crust Index (TCI); (B) The central dune incursion corridor. Imposed on top are the ASTER and DAIS bands used in the formulation of the Thermal Crust Index (TCI).

2.4. Airborne images

DAIS-7915 images were acquired over Israel on August 2nd 1997 around noontime (Ben-Dor et al., 2002). The image we processed is of an area over the Negev Desert, close to the border at the southern dune incursion corridor. The sensor is a hyperspectral sensor for the VIS-NIR-SWIR region with 72 spectral bands between 0.5 and 2.5 μm. In the TIR region, the sensor has seven multispectral bands, out of which six are in the LWIR. Unfortunately, calibration of the DAIS image taken over the research area in the northwestern Negev

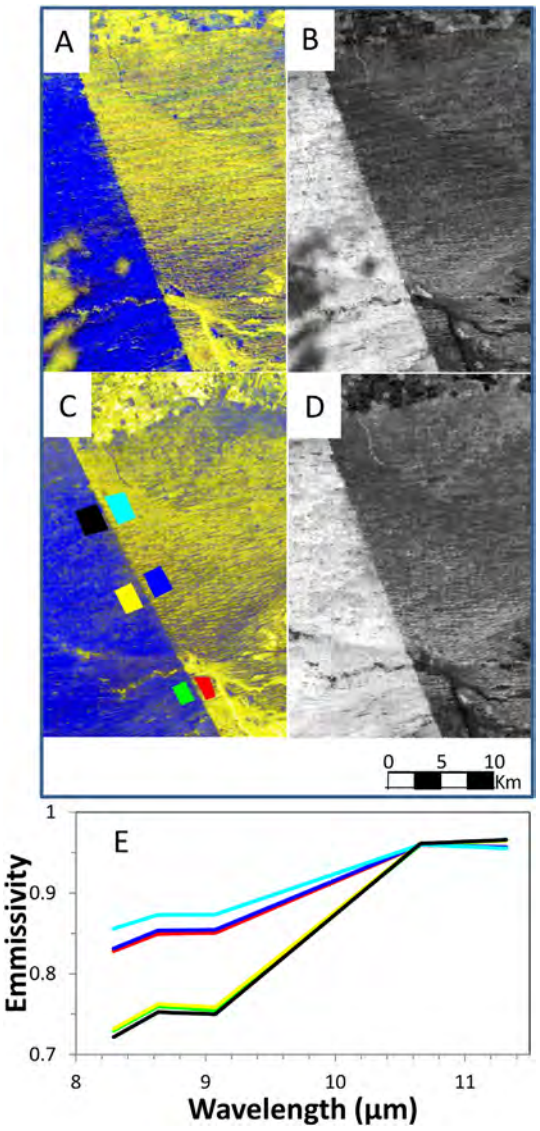

Fig. 4. (A) ASTER-derived night surface emissivity (Sep. 20, 2005, RGB = 11,12,14); (B) Thermal Crust Index (TCI) derived from Fig. 4A; (C) ASTER-derived day surface emissivity (Oct. 23, 2004, RGB = 11,12,14). The polygon pairs were chosen from each of the three dune incursion corridors in order to compare the spectral signatures of both sides of the border; (D) TCI for day time derived from Fig. 4C; (E) Emissivity signature comparison according to the polygons marked on the image in Fig. 4C. The polygons on the Egyptian side of the border display very similar spectral emissivity signatures that are lower than those displayed on the Israeli side of the border.

dunes was not achieved due to issues with the instrument calibration to radiance, and the lack of ground spectral measurements during the time of image acquisition. As a result, the DAIS image was processed as raw digital numbers (DN) data without calibrating them to reflectance and emissivity. Therefore, we will treat these data as a visualization aid, and use them to perform categorical classification, rather than for chemometrics. The Crust Index (CI) (Karnieli, 1997), Normalized-Difference Vegetation Index (NDVI) (Tucker, 1979), and the newly formalized TCI were applied to the DAIS image. Five land-cover classes (pebbles, playa, sand, vegetation, and BSCs) were classified from each combination of the indices, using a maximum likelihood classifier.

A set of 500 randomly sampled points was interpreted from an orthophoto and used for an accuracy assessment of the classification products. Each classification product was assessed using an error matrix (Congalton and Green, 2008). Accuracy measures, such as overall accuracy and Kappa statistic, were calculated for every error matrix. To assess the accuracy of specific categories, we calculated the user's accuracy, producer's accuracy, and the conditional Kappa coefficient. We used the approximate large sample variance of both the Kappa statistic and the conditional Kappa statistic for every category to estimate their variance. The variance estimations were used to calculate confidence intervals, and to determine if one classification is significantly more accurate than another by performing a two-tailed Z-test with $\alpha = 0.05$.

3. Results and discussion

3.1. Emissivity signatures of BSCs from ground spectral measurements

The spectral emissivity of bare sand, physical crust from playa, and of several BSC types from the southern dune incursion corridor are presented in Fig. 3A. Apparently, sand has the lowest emissivity.

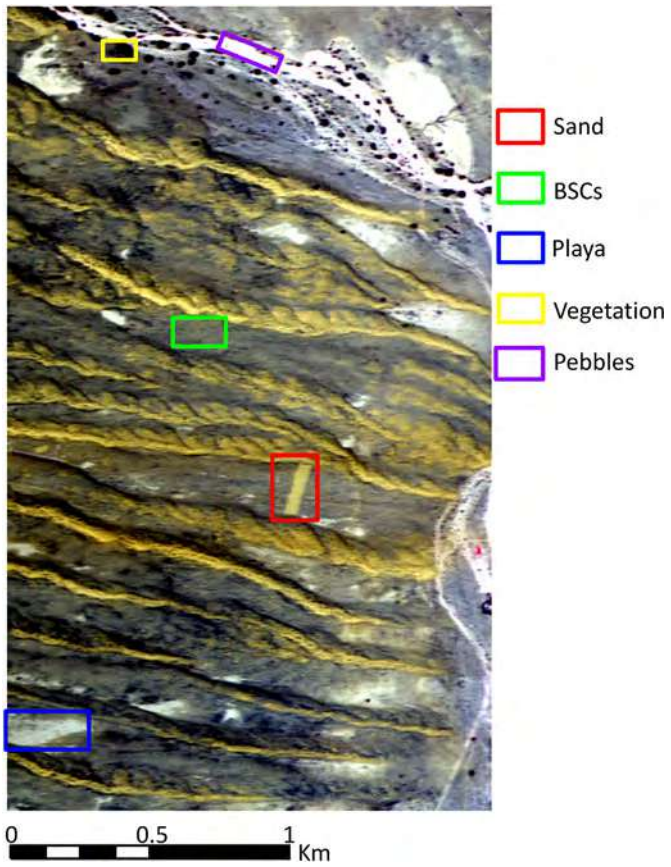

Fig. 5. False color composite of DAIS (RGB = 18,10,1, NIR, red, green). The frames on the image are examples of each of the five main classes of land cover. The sand example is of a scar made by a tractor that scraped the interdune area the day before the image was acquired. The tractor removed the BSCs from that portion of the image, and exposed the sand underneath them; therefore, the pixels in that area are of pure bare sand. Other pure sand pixels can be found on the dune crests, stretching from west to east. Limestone pebbles are found on the bottom of the wadi (crossing at the top of the scene). Vegetation patches are found all over the scene: on dune crests, on the dune slopes, and interdune areas. The largest and most obvious vegetation patches are in and around the wadi. Playas occupy some of the interdune spaces where highly carbonatic paludal loam sediments were deposited due to dunes damming the wadi, creating the water ponds. This whitish-gray paludal sediment has a distinct spectral-mineralogical signature that contrasts with the surrounding sand and BSCs. (For interpretation of the references to color in this figure legend, the reader is referred to the web version of this article.)

This finding corroborates findings by Qin et al. (2002) who showed that sand has a lower emissivity than BSCs. Our hyperspectral measurements add to the mono-band measurements performed by Qin et al. (2002) by enhancing specific spectral features. The main quartz feature in this range is a doublet at 8–10 μm. At this range, all BSC samples still possess the doublet feature, but its depth differs: BSCs of the southern face and the interdune area, which are the least developed BSCs, display emissivity in the mid-range between the sand and the well-developed BSCs of the northern face. It appears that as the crust grows more developed and gains more biomass, it attenuates the signal from the quartz grains. The physical crust extracted from the playa shows a similar effect, since it is composed of clay minerals. Therefore, the clay particles on the surface of the playa display a higher emissivity than the silicate sand of the dune crest. This difference between quartz and clay minerals corroborates the findings of Vaughan et al. (2003) who showed this difference in hyperspectral LWIR imagery.

The spectral emissivity values of bare sand and several BSC types from the central dune incursion corridor are presented in Fig. 3B. These BSCs are more mature and developed than the BSCs of the southern corridor, and their emissivity values are accordingly higher, when comparing the same aspects of both locations. However, when we compare the different aspects of the central incursion corridor, we observe the same trend as in the southern corridor: sand presents the lowest emissivity with a clear doublet that is attenuated in BSC samples in direct relation to the BSCs' level of development. The least developed BSCs of the southern slope present emissivity values in the mid-range between the sand and the well-developed BSCs of the northern slopes. The emissivity spectrum from BSCs of the interdune areas is similar to the emissivity signature of BSCs from the southern slope, but slightly higher. BSCs from the northern slopes present two types of patches: those that are dominated by cyano-lichens, and those that are dominated by moss. Both BSC types show very high emissivity values, with almost complete masking of the quartz doublet feature.

This ability to determine the succession trends of microphytic communities and to rank BSCs on these scales opens the door for ecological applications. Knowledge regarding the effects of BSCs' community composition on various ecosystem functions could be used to model these functions with respect to soil surface spectra. For instance, once models are derived, functions, such as ground stabilization and mechanical properties, could be estimated from the spectra, without the need for any destructive analysis. Another possible use for spectral knowledge coupled with ecosystem functions is the mapping of different habitats within an ecosystem based on the surface spectra. While these applications exceed the scope of this paper, future studies might employ the techniques presented here for similar purposes.

3.2. Implementation of Thermal Crust Index (TCI)

Our goal was to create a spectral index for the discrimination of sand and BSCs of different types that can be successfully applied to multispectral remote sensing LWIR data. It became apparent that the slope between the emissivity minimum at 8.8 μm and the shoulder feature at 10.2 μm changes according to the BSCs' level of development with a very high slope for sand and gradually decreasing slopes, as BSC becomes more mature. This discriminative slope feature remained even when the hyperspectral resolution was degraded to a DAIS or ASTER resolution. Therefore, we used two multispectral bands centered at the two ends of this slope to define a normalized difference index:

$$TCI = \frac{\varepsilon_1 - \varepsilon_2}{\varepsilon_1 + \varepsilon_2} \quad (3)$$

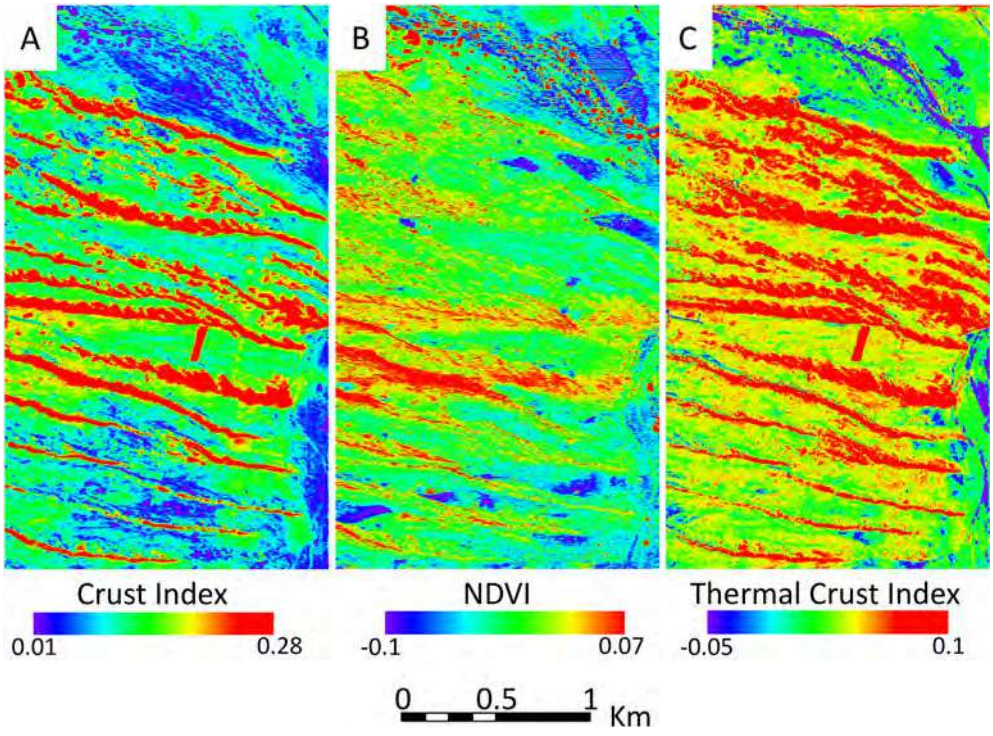

Fig. 6. (A) Crust index (CI); (B) Normalized Difference Vegetation Index (NDVI); (C) Thermal Crust Index (TCI). CI and TCI both discriminate sand from Biological Soil Crusts (BSCs) well, but they differ in their ability to discriminate between other classes. While both CI and TCI only moderately discriminate between vegetation and playas, the NDVI is able to perform this discrimination much better. TCI also identifies limestone pebbles very well. Note that for the purpose of presentation, high values in both CI and TCI signify low crust signal.

where ε_1 and ε_2 for ASTER are the emissivity at bands 13 and 12, respectively. When implementing the index for the uncalibrated DAIS image, we used the DN values for bands 76 and 75, respectively. Fig. 3A and B show the spectral resolution difference between the ASTER and DAIS bands. The ASTER bands are wide and slightly overlap, while the DAIS bands are narrower with no overlap.

3.3. Regional scale emissivity measurements using ASTER thermal imagery

The contrast in the emissivity spectrum between the two sides of the border is demonstrated for both day and night images. When the TCI is implemented for the ASTER images, the contrast between the two sides of the border is very clear for both day and night images (Fig. 4). This is an advantage of multispectral emissivity products over temperature products. It was previously demonstrated by Qin et al. (2002) that the temperature contrast disappears during the night. However, the emissivity contrast remains, day and night, as we demonstrate here.

When comparing the two sides of the border (Figs. 4C and E), we demonstrate that the Egyptian side presents lower emissivity than the Israeli side. This is expected, as most of the surface in Sinai is covered by bare sand, and most of the surface in the Negev is covered by BSCs. The contribution of vascular vegetation to the emissivity contrast is assumed to be lesser than that of BSC cover, since the vegetation cover is very low on both sides. The slightly higher amount of vegetation cover in the Negev, relative to the cover in Sinai (Qin et al., 2006; Seifan, 2009), could contribute to the higher Negev emissivity values. The three polygons on the Egyptian side present very similar signatures, while the northern Negev polygon presents a slightly higher emissivity than the central and southern polygons. We propose two drivers for the higher emissivity in the northern Negev: first, the BSCs are of later successional stages as precipitation increases towards the northern section of the research area. Thus, the BSCs in the north have a higher emissivity. Second, the proportions of land-cover components change in such a way that they affect the polygon signature: i.e., a larger fraction of BSCs and less bare sand. In addition, the dune morphology in the northern incursion corridor is significantly different and leads to a smaller proportion of exposed active sand. Higher precipitation could also lead to an increase in vacuolar vegetation coverage. However, Siegal et al. (2013) show that the vegetation cover amounts in both the northern and central incursion corridors are similar (10–20%), while in the southern corridor, the vegetation cover is lower (5–13%). Therefore, we are able to exclude the differences in vascular vegetation cover as a cause for the emissivity difference between the northern and central corridors. We are able to show that the spectral differences between the two sides of the border, as measured by satellite, are as expected and correspond well to our ground sample measurements.

3.4. Data fusion of different spectral regions from DAIS imagery for land-cover classification

The DAIS image has a spatial resolution of 1 m^2, and therefore, we can recognize and discriminate specific objects, such as vegetation patches, dune crests, roads, wadis, etc. Fig. 5 displays a false color composite of the DAIS scene with specific regions of interest pertaining to the five main land-cover classes in the scene. The footprint of this image is marked in Fig 1B. Unlike classic false color composites, the vegetation in this image is not displayed in red. This phenomenon was explained by Pinker and Karnieli (1995) who showed that the NIR spectral reflectance of desert perennial bushes is very low in comparison to the green vegetation of non-arid regions (Pinker and Karnieli, 1995). At the time of the DAIS image acquisition towards the end of the summer, these desert bushes appeared in grayish-green tones and not vibrant green as is the vegetation in non-arid areas. The red rectangle in Fig. 5 is a strip of bare sand, uncovered by a tractor that scraped the interdune area on the day before the flight, thus removing all of the BSC from the surface. Fig. 6 displays the three indices: CI, NDVI, and TCI. Each of these indices excels at enhancing different cover types. While both CI and TCI enhance the discrimination of sand from BSCs, it appears that CI can help to recognize vegetation patches slightly better than TCI. However, TCI has the ability to distinguish the limestone pebbles at the wadi infrastructure. NDVI seems to excel at enhancing the vegetation signal and also at distinguishing playas from their surroundings. A combination of all three indices into one image that serves as a visualization

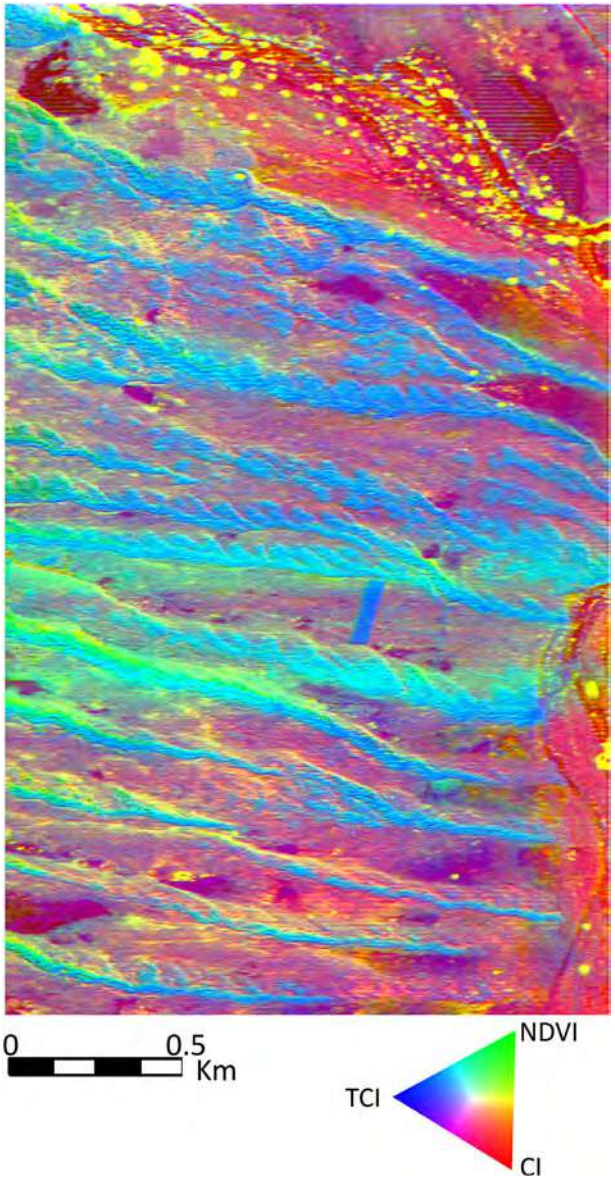

Fig. 7. Pseudo-color map showing the relative distribution of CI, NDVI, and TCI within the domain. The meaning of the colors is given in a ternary diagram. This band combination is particularly useful for visually discriminating between the different land-cover classes: vegetation patches are shown as yellow, pebbles as red, playa as purple, Biological Soil Crust (BSCs) appear in pink, and sand in blue. (For interpretation of the references to color in this figure legend, the reader is referred to the web version of this article.)

Table 1
Error matrices for classification of: (A) CI + NDVI + TCI; (B) CI + NDVI; (C) NDVI + TCI; (D) CI + TCI; (E) CI; (F) NDVI; (G) TCI.

	Pebbles	Playa	BSC	Vegetation	Sand	Sum	User's accuracy
A							
Pebbles	*55*	29	13	3	0	**100**	55.00%
Playa	8	*82*	8	1	1	**100**	82.00%
BSC	1	0	*99*	0	0	**100**	99.00%
Vegetation	0	0	2	*98*	0	**100**	98.00%
Sand	0	1	2	0	*97*	**100**	97.00%
Sum	**64**	**112**	**124**	**102**	**98**	***431***	
Producer's accuracy	85.94%	73.87%	79.84%	96.08%	98.98%		
B							
Pebbles	*41*	40	43	60	16	**200**	20.50%
Playa	8	*36*	7	6	6	**63**	57.14%
BSC	7	16	*66*	9	6	**104**	63.46%
Vegetation	3	7	2	*16*	3	**31**	51.61%
Sand	5	13	6	11	*67*	**102**	65.69%
Sum	**64**	**112**	**124**	**102**	**98**	***226***	
Producer's accuracy	64.06%	32.14%	53.23%	15.69%	68.37%		
C							
Pebbles	*15*	10	2	15	5	**47**	31.91%
Playa	28	*55*	25	37	10	**155**	35.48%
BSC	3	10	*78*	5	7	**103**	66.00%
Vegetation	13	27	10	*35*	10	**95**	36.84%
Sand	5	10	9	10	*66*	**100**	75.73%
Sum	**64**	**112**	**124**	**102**	**98**	***249***	
Producer's accuracy	23.44%	49.11%	67.35%	34.31%	62.90%		
D							
Pebbles	*22*	16	5	18	6	**67**	32.84%
Playa	17	*57*	29	27	11	**141**	40.43%
BSC	9	19	*81*	12	3	**124**	70.00%
Vegetation	11	9	5	*35*	8	**68**	51.47%
Sand	5	11	4	10	*70*	**100**	65.32%
Sum	**64**	**112**	**124**	**102**	**98**	***265***	
Producer's accuracy	34.38%	50.89%	71.43%	34.31%	65.32%		
E							
Pebbles	*36*	29	40	60	13	**178**	20.22%
Playa	7	*28*	39	5	7	**86**	32.56%
BSC	14	37	*35*	16	6	**108**	64.15%
Vegetation	2	4	2	*10*	4	**22**	45.45%
Sand	5	14	8	11	*68*	**106**	32.41%
Sum	**64**	**112**	**124**	**102**	**98**	***177***	
Producer's accuracy	56.25%	25.00%	69.39%	9.80%	28.23%		
F							
Pebbles	*23*	40	50	34	14	**161**	14.29%
Playa	14	*25*	5	10	5	**59**	42.37%
BSC	6	6	*15*	9	6	**42**	34.27%
Vegetation	5	19	4	*20*	12	**60**	33.33%
Sand	16	22	50	29	*61*	**178**	35.71%
Sum	**64**	**112**	**124**	**102**	**98**	***144***	
Producer's accuracy	35.94%	22.32%	62.24%	19.61%	12.10%		
G							
Pebbles	*9*	4	0	12	3	**28**	32.14%
Playa	29	*62*	61	61	25	**238**	26.05%
BSC	4	12	*49*	6	4	**75**	66.67%
Vegetation	18	24	7	*13*	4	**66**	19.70%
Sand	4	10	7	10	*62*	**93**	65.33%
Sum	**64**	**112**	**124**	**102**	**98**	***195***	
Producer's accuracy	14.06%	55.36%	63.27%	12.75%	39.52%		

Overall Classification Accuracy (A) = 86.20%.
Overall Classification Accuracy (B) = 45.20%.
Overall Classification Accuracy (C) = 49.80%.
Overall Classification Accuracy (D) = 53.00%.
Overall Classification Accuracy (E) = 35.40%.
Overall Classification Accuracy (F) = 28.80%.
Overall Classification Accuracy (G) = 39.00%.
The sum of rows and columns are marked in bold. Correctly classified samples are marked in italics. The total sum of all correctly classified samples are underlined.

aid is presented in Fig 7. The three-index composite greatly enhances our ability to discern the different land-cover classes.

To quantify the advantage of each index by itself and of every index combination, we have classified each index combination. Confusion matrices for the classification of every index combination are presented in Table 1. Classification accuracy measurements, in the form of an overall Kappa statistic and a conditional Kappa statistic with 95% confidence intervals of all the index combinations, are presented in Fig. 8. A complementary analysis of *Z*-tests for every pair of overall Kappa statistics and conditional Kappa statistics, to determine whether they are significantly different from each other, is presented in Table 2. The results indicate that a combination of all three indices is always significantly better in terms of classification accuracy than any other index combination. TCI is superior to each of

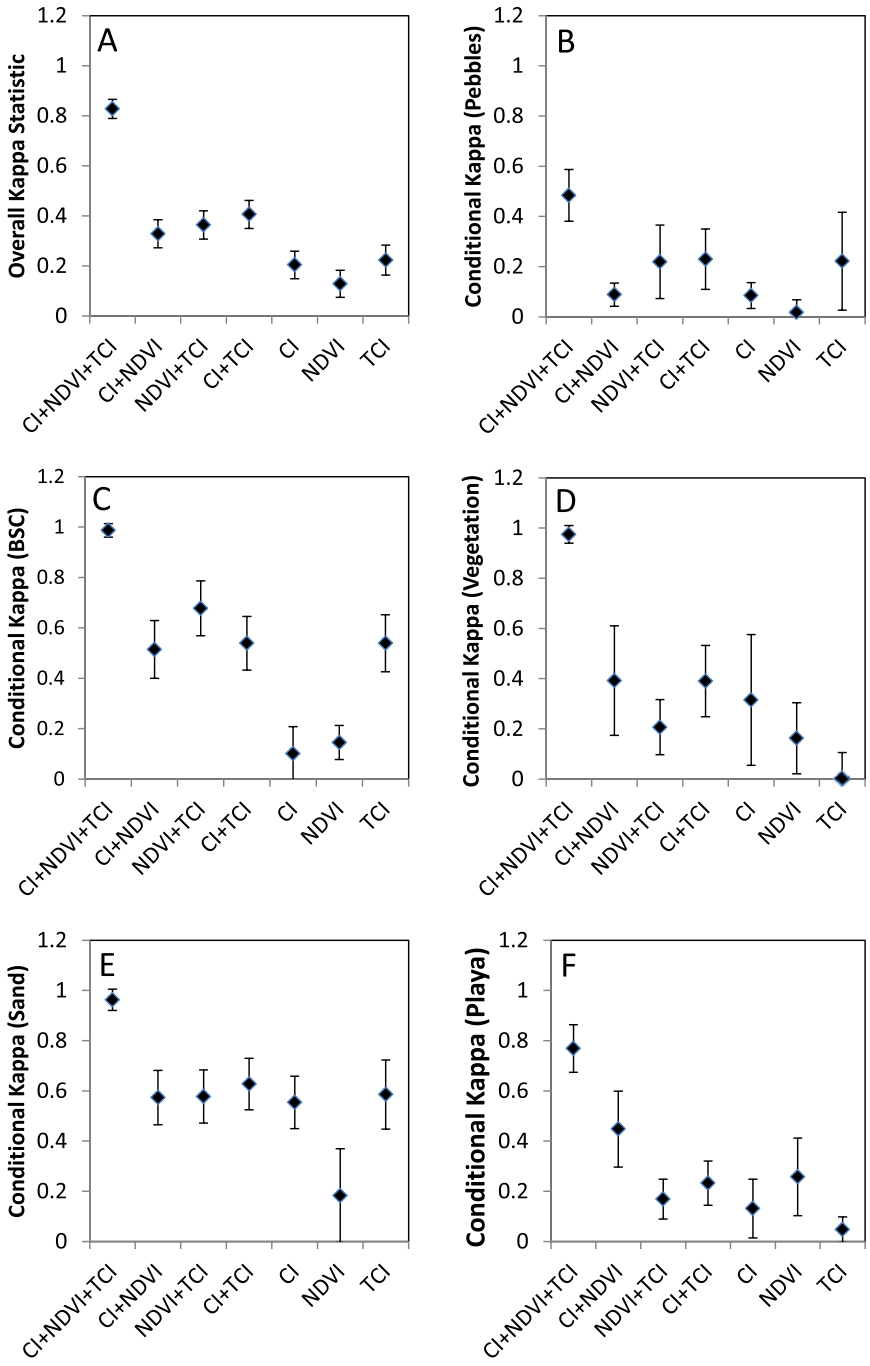

Fig. 8. Accuracy measures for entire error matrices (A) and for specific classes (B–F). The error bars represent a 95% confidence interval. The overall Kappa statistic represents the accuracy of the entire error matrix in comparison to a random error matrix, or a random classification. The conditional Kappa statistic represents the accuracy of a single class.

the other two indices separately for the classification of BSCs. The combinations of TCI with NDVI or CI yield similar BSC classification accuracy to NDVI + CI and to TCI by itself. The combination of all three indices is synergetic since near perfect accuracy is achieved for BSC classification. Other results are obtained for the vegetation class: NDVI is not significantly more accurate than each of the other indices by itself, or the combinations of NDVI with each of them. However, the combination of CI + TCI is more accurate for the vegetation class than NDVI by itself, and similar in accuracy to NDVI + TCI and CI + NDVI. The similarity between the vegetation class and the BSC class is expressed by the synergy between all three indices that leads to near perfect classification accuracy in the vegetation class. The sand class is characterized by low classification accuracy when classifying NDVI, and medium classification accuracy for all other combinations except for the three-index combination that results in near perfect classification accuracy. Pebbles and playa are the two least accurately classified categories, as they are often misclassified, with great confusion between each other in all classifications. These two land-covers types are the brightest in the scene, and it is possible that another classification method could have achieved better accuracy for them as well. More spectral information, such as a hyperspectral SWIR-based index, might prove to be beneficial for this task, since the signatures of calcite and different clay minerals differ in that spectral region. Regrettably, the

Table 2
Results of *Z*-tests for determination of whether the individual confusion matrices are different from one another: (A) overall Kappa statistic; (B) conditional Kappa statistic of the pebble class; (C) conditional Kappa statistic of the playa class; (D) conditional Kappa statistic of the Biological Soil Crust (BSC) class; (E) conditional Kappa statistic of the vegetation class; (F) conditional Kappa statistic of the sand class. Each value in the matrices represents the test statistic for a single *Z*-test conducted between classification of the index combinations listed in the row and column margins. Significant results for $\alpha = 0.05$ are marked in bold.

	CI + NDVI + TCI	CI + NDVI	NDVI + TCI	CI + TCI	CI	NDVI	TCI
A							
CI + NDVI + TCI	**						
CI + NDVI	**14.72**	**					
NDVI + TCI	**13.60**	0.89	**				
CI + TCI	**12.44**	1.95	1.06	**			
CI	**18.58**	**3.17**	**4.06**	**5.14**	**		
NDVI	**21.07**	**5.14**	**6.02**	**7.12**	1.95	**	
TCI	**17.03**	**2.57**	**3.42**	**4.46**	0.47	**2.35**	**
B							
CI + NDVI + TCI	**						
CI + NDVI	**7.00**	**					
NDVI + TCI	**2.95**	1.70	**				
CI + TCI	**3.21**	**2.20**	0.11	**			
CI	**6.92**	0.09	1.73	**2.21**	**		
NDVI	**8.11**	**2.07**	**2.61**	**3.26**	1.88	**	
TCI	**2.37**	1.33	0.02	0.07	1.35	**2.03**	**
C							
CI + NDVI + TCI	**						
CI + NDVI	**3.59**	**					
NDVI + TCI	**9.68**	**3.26**	**				
CI + TCI	**8.27**	**2.46**	1.07	**			
CI	**8.47**	**3.31**	0.53	1.39	**		
NDVI	**5.63**	1.76	1.02	0.28	1.31	**	
TCI	**13.39**	**5.02**	**2.57**	**3.64**	1.32	**2.58**	**
D							
CI + NDVI + TCI	**						
CI + NDVI	**8.02**	**					
NDVI + TCI	**5.52**	**2.06**	**				
CI + TCI	**8.17**	0.32	1.82	**			
CI	**16.19**	**5.28**	**7.57**	**5.82**	**		
NDVI	**23.18**	**5.53**	**8.29**	**6.25**	0.70	**	
TCI	**7.70**	0.31	1.76	0.00	**5.64**	**5.97**	**
E							
CI + NDVI + TCI	**						
CI + NDVI	**5.27**	**					
NDVI + TCI	**13.32**	1.52	**				
CI + TCI	**8.01**	0.01	**2.05**	**			
CI	**5.02**	0.45	0.77	0.51	**		
NDVI	**11.12**	1.76	0.49	**2.27**	1.03	**	
TCI	**16.39**	**3.25**	**2.71**	**4.37**	**2.27**	1.88	**
F							
CI + NDVI + TCI	**						
CI + NDVI	**6.72**	**					
NDVI + TCI	**6.77**	0.05	**				
CI + TCI	**6.05**	0.72	0.68	**			
CI	**7.26**	0.25	0.31	0.99	**		
NDVI	**8.13**	**3.62**	**3.67**	**4.16**	**3.47**	**	
TCI	**5.24**	0.14	0.10	0.48	0.36	**3.47**	**

DAIS SWIR bands are too noisy to extract this spectral data. Nevertheless, the three-index combination exhibited its synergetic qualities with classification accuracy for the pebble and playa classes as well, being significantly more accurate than any other index combination. Since this combination is repeatedly better than any other combination for all classes, we can conclude that fusion of the different spectral regions provides complementary information that improves our classification abilities in this desert environment.

4. Summary and conclusions

- High spectral resolution measurements of BSCs, sand, and physical crust were characterized. It was found that BSCs have different spectral signatures than silicate sand in the LWIR spectral region. It was demonstrated that as BSCs' succession advances and the microphytic community is more mature, the quartz doublet at the area of 8–10 μm is attenuated. It was also demonstrated that this feature was attenuated for physical crust, since physical crusts are composed of fine particles of clay minerals.
- The ability to rank BSCs' successional maturity, using spectroscopy, may lead to the modeling of ecosystem functions and the estimation of parameters from spectroscopic measurements, in a non-destructive manner.
- TCI was developed for use with multispectral remote sensing LWIR data to discriminate sand from BSCs of different maturity levels. While it is clear that TCI serves well to discriminate between sand and BSC, we have only been able to show its abilities to classify different BSCs using ground spectroscopy. We have not been able to upscale that ability and show that TCI can discriminate between different types of BSCs using remote sensing imagery, since the DAIS image was not radiometrically calibrated, and the pixel size of the ASTER image is too coarse. It

is expected that future studies, using LWIR images of better radiometric quality and a higher spatial resolution, would be able to successfully classify several BSC types.

- TCI was compared with CI in the same desert dune environment in which CI was developed. It was found that TCI enhances the signals of BSCs and of limestone pebbles more than CI, while CI was slightly more sensitive for vegetation. CI and TCI equally enhanced the signal of sand. They were both found to be relatively insensitive to the signals of physical crusts at the playa surface.
- The fusion of information from different spectral regions was proven to be extremely productive, as each spectral region contains complementary information, and their combination greatly enhances our ability to perform a surface cover analysis. The combination of CI and TCI that are suitable for enhancing the signals of BSCs, sand, and limestone pebbles, with NDVI that is suitable for enhancing vegetation and playa signals enables very accurate land-cover classification, especially for BSC, sand, and vegetation classes.
- Presentation of CI, NDVI, and TCI as a pseudo-color image is very convenient for land-cover interpretation and analysis.
- LWIR multispectral remote sensing can be used to measure differences in emissivity, even at night, when temperature differences subside and reflective remote sensing is not relevant.
- The main advantage of increased spectral resolution in the LWIR region is the ability to obtain emissivity signatures, which are unaffected by environmental variables, as opposed to temperature data that may depend on the time of day and the season.

Acknowledgments

The project was funded by the Israeli Ministry of Science and Technology. Offer Rozenstein was supported by the Pratt Foundation. The authors wish to thank Gila Notesco, Amir Gil, Vered Ben-Yaacov, and Tal Katz for their assistance in SR-5000 measurements and processing. Simon Berkowicz of the Arid Ecosystem Research Center (AERC) and Zehava Sigal are thanked for sharing precipitation data. Joel Roskin is thanked for lengthy discussions about the research area.

References

Bamforth, S.S., 2008. Protozoa of biological soil crusts of a cool desert in Utah. J. Arid. Environ. 72, 722–729.
Belnap, J., 2006. The potential roles of biological soil crusts in dryland hydrologic cycles. Hydrol. Process 20, 3159–3178.
Belnap, J., Eldridge, D., 2001. Disturbance and recovery of biological soil crusts. In: Belnap, J., Lange, O.L. (Eds.), Biological Soil Crusts: Structure, Function, and Management. Springer-Verlag, Berlin, pp. 363–383.
Belnap, J., Phillips, S.L., Witwicki, D.L., Miller, M.E., 2008. Visually assessing the level of development and soil surface stability of cyanobacterially dominated biological soil crusts. J. Arid. Environ. 72, 1257–1264.
Ben-David, E.A., Zaady, E., Sher, Y., Nejidat, A., 2011. Assessment of the spatial distribution of soil microbial communities in patchy arid and semi-arid landscapes of the Negev Desert using combined PLFA and DGGE analyses. FEMS Microbiol. Ecol. 76, 492–503.
Ben-Dor, E., Patkin, K., Banin, A., Karnieli, A., 2002. Mapping of several soil properties using DAIS-7915 hyperspectral scanner data – a case study over clayey soils in Israel. Int. J. Remote Sens. 23, 1043–1062.
Boeken, B., Ariza, C., Gutterman, Y., Zaady, E., 2004. Environmental factors affecting dispersal, germination and distribution of Stipa capensis in the Negev Desert, Israel. Ecol. Res. 19, 533–540.
Bowker, M.A., 2007. Biological soil crust rehabilitation in theory and practice: an underexploited opportunity. Restor. Ecol. 15, 13–23.
Büdel, B., Veste, M., 2008. Biological crusts. In: Breckle, S., Yair, A., Veste, M. (Eds.), Arid Dune Ecosystems; the Nizzana Sands in the Negev Desert. Springer, Berlin, pp. 149–155.
Burgheimer, J., Wilske, B., Maseyk, K., Karnieli, A., Zaady, E., Yakir, D., Kesselmeier, J., 2006. Relationships between Normalized Difference Vegetation Index (NDVI) and carbon fluxes of biologic soil crusts assessed by ground measurements. J. Arid Environ. 64, 651–669.
Cabib, D., Gil, A., Buckwald, R.A., 2004. New user interface and features of the SR 5000: revival of infrared CVF based spectroradiometry. Proc. SPIE 5431, 47.
Chen, J., Yuan Zhang, M., Wang, L., Shimazaki, H., Tamura, M., 2005. A new index for mapping lichen-dominated biological soil crusts in desert areas. Remote Sens. Environ. 96, 165–175.
Collins, B.H., 1996. Thermal Imagery Spectral Analysis (Master's thesis). Naval Postgraduate School Monterey, California.
Congalton, R.G., Green, K., 2008. Assessing the Accuracy of Remotely Sensed Data: Principles and Practices. Lewis Publishers, Boca Raton.
Darby, B.J., Neher, D.A., Belnap, J., 2007. Soil nematode communities are ecologically more mature beneath late- than early-successional stage biological soil crusts. Appl. Soil Ecol. 35, 203–212.
Eisele, A., Lau, I., Hewson, R., Carter, D., Wheaton, B., Ong, C., Cudahy, T.J., Chabrillat, S., Kaufmann, H., 2012. Applicability of the Thermal infrared spectral region for the prediction of soil properties across semi-arid agricultural landscapes. Remote Sens. 4, 3265–3286.
Gillespie, A., Rokugawa, S., Matsunaga, T., Cothern, J.S., Hook, S., Kahle, A.B., 1998. A temperature and emissivity separation algorithm for advanced spaceborne thermal emission and reflection radiometer (ASTER) images. Geosci. Remote Sens. IEEE Trans. 36, 1113–1126.
Guo, Y., Zhao, H., Zuo, X., Drake, S., Zhao, X., 2008. Biological soil crust development and its topsoil properties in the process of dune stabilization, Inner Mongolia, China. Environ. Geol. 54, 653–662.
Horton, K.A., Johnson, J.R., Lucey, P.G., 1998. Infrared measurements of pristine and disturbed soils 2. Environmental effects and field data reduction. Remote Sens. Environ. 64, 47–52.
Housman, D., Powers, H., Collins, A., Belnap, J., 2006. Carbon and nitrogen fixation differ between successional stages of biological soil crusts in the Colorado Plateau and Chihuahuan Desert. J. Arid Environ. 66, 620–634.
Jimenez Aguilar, A., Huber-Sannwald, E., Belnap, J., Smart, D., Arredondo Moreno, J., 2009. Biological soil crusts exhibit a dynamic response to seasonal rain and release from grazing with implications for soil stability. J. Arid Environ. 73, 1158–1169.
Kahle, A.B., Goetz, A.F.H., 1983. Mineralogic information from a new airborne thermal infrared multispectral scanner. Science 222, 24.
Kahle, A.B., Palluconi, F.D., Hook, S.J., Realmuto, V.J., Bothwell, G., 1991. The advanced spaceborne thermal emission and reflectance radiometer (Aster). Int. J. Imaging Syst. Technol. 3, 144–156.
Karnieli, A., 2003. Natural vegetation phenology assessment by ground spectral measurements in two semi-arid environments. Int. J. Biometeorol. 47, 179–187.
Karnieli, A., Dall'Olmo, G., 2003. Remote-sensing monitoring of desertification, phenology, and droughts. Manag. Environ. Qual. Int. J. 14, 22–38.
Karnieli, A., Gabai, A., Ichoku, C., Zaady, E., Shachak, M., 2002. Temporal dynamics of soil and vegetation spectral responses in a semi-arid environment. Int. J. Remote Sens. 23, 4073–4087.
Karnieli, A., Kidron, G.J., Glaesser, C., Ben-Dor, E., 1999. Spectral characteristics of cyanobacteria soil crust in semiarid environments. Remote Sens. Environ. 69, 67–75.
Karnieli, A., 1997. Development and implementation of spectral crust index over dune sands. Int. J. Remote Sens. 18, 1207–1220.
Karnieli, A., Tsoar, H., 1995. Satellite spectral reflectance of biogenic crust developed on desert dune sand along the Israel–Egypt border. Int. J. Remote Sens. 16, 369–374.
Karnieli, A., Kokaly, R., West, N.E., Clark, R.N., 2001. Remote sensing of biological soil crusts. In: Belnap, J., Lange, O. (Eds.), Biological Soil Crusts: Structure, Function, and Management. Springer-Verlag, Berlin, pp. 431–455.
Kirkland, L., Herr, K., Keim, E., Adams, P., Salisbury, J., Hackwell, J., Treiman, A., 2002. First use of an airborne thermal infrared hyperspectral scanner for compositional mapping. Remote Sens. Environ. 80, 447–459.
Magaritz, M., Enzel, Y., 1990. Standing-water deposits as indicators of Late Quaternary dune migration in the northwestern Negev, Israel. Clim. Change 16, 307–318.
Milton, E.J., Schaepman, M.E., Anderson, K., Kneubühler, M., Fox, N., 2009. Progress in field spectroscopy. Remote Sens. Environ. 113, S92–S109.
Moghtaderi, A., Moore, F., Taghavi, S., Rezaei, R., 2011. The application of ASTER imageries and mathematical evaluation method in detecting cyanobacteria in biological soil crust, Chadormalu area, central Iran. Iran. J. Sci. Technol. 1, 13–28.
Pinker, R.T., Karnieli, A., 1995. Characteristic spectral reflectance of a semi-arid environment. Int. J. Remote Sens. 16, 1341–1363.
Qin, Z., Berliner, P., Karnieli, A., 2002. Micrometeorological modeling to understand the thermal anomaly in the sand dunes across the Israel–Egypt border. J. Arid Environ. 51, 281–318.
Qin, Z., Berliner, P., Karnieli, A., 2005. Ground temperature measurement and emissivity determination to understand the thermal anomaly and its significance on the development of an arid environmental ecosystem in the sand dunes across the Israel–Egypt border. J. Arid Environ. 60, 27–52.
Qin, Z., Dall'Olmo, G., Karnieli, A., Berliner, P., 2001. Derivation of split window algorithm and its sensitivity analysis for retrieving land surface temperature from NOAA-advanced very high resolution radiometer data. J. Geophys. Res. 106, 22655–22670.
Qin, Z., Li, W., Burgheimer, J., Karnieli, A., 2006. Quantitative estimation of land cover structure in an arid region across the Israel–Egypt border using remote sensing data. J. Arid Environ. 66, 336–352.
Ribeiro da Luz, B., Crowley, J.K., 2010. Identification of plant species by using high spatial and spectral resolution thermal infrared (8.0–13.5 μm) imagery. Remote Sens. Environ. 114, 404–413.

Ribeiro da Luz, B., Crowley, J.K., 2007. Spectral reflectance and emissivity features of broad leaf plants: prospects for remote sensing in the thermal infrared (8.0–14.0 μm). Remote Sens. Environ. 109, 393–405.
Roskin, J., Blumberg, D.G., Porat, N., Tsoar, H., Rozenstein, O., 2011a. Do dune sands redden with age? The case of the northwestern Negev dunefield, Israel. Aeolian Res. 5, 63–75.
Roskin, J., Porat, N., Tsoar, H., Blumberg, D.G., Zander, A.M., 2011b. Age, origin and climatic controls on vegetated linear dunes in the northwestern Negev Desert (Israel). Quat. Sci. Rev. 30 (13–14), 1649–1674.
Salisbury, J.W., D'Aria, D.M., 1992. Emissivity of terrestrial materials in the 8–14 μm atmospheric window. Remote Sens. Environ. 42, 83–106.
Salisbury, J.W., Wald, A., 1992. The role of volume scattering in reducing spectral contrast of reststrahlen bands in spectra of powdered minerals. Icarus 96, 121–128.
Schaepman, M.E., Ustin, S.L., Plaza, A.J., Painter, T.H., Verrelst, J., Liang, S., 2009. Earth system science related imaging spectroscopy—an assessment. Remote Sens. Environ. 113 (Suppl. 1), S123–S137.
Seifan, M., 2009. Long-term effects of anthropogenic activities on semi-arid sand dunes. J. Arid Environ. 73, 332–337.
Serpe, M., Orm, J., Barkes, T., Rosentreter, R., 2006. Germination and seed water status of four grasses on moss-dominated biological soil crusts from arid lands. Plant Ecol. 185, 163–178.
Siegal, Z., Tsoar, H., Karnieli, A., 2013. Effects of prolonged drought on the vegetation cover of sand dunes in the NW Negev Desert: field survey, remote sensing and conceptual modeling. Aeolian Res. 9, 161–173.
Tsoar, H., Blumberg, D.G., Wenkart, R., 2008. Formation and geomorphology of the North-Western Negev sand dunes. In: Breckle, S., Yair, A., Veste, M. (Eds.), Arid Dune Ecosystems the Nizzana Sands in the Negev Desert. Springer, Berlin Heidelberg, pp. 25–48.
Tsoar, H., Karnieli, A., 1996. What determines the spectral reflectance of the Negev–Sinai sand dunes. Int. J. Remote Sens. 17, 513–525.
Tucker, C.J., 1979. Red and photographic infrared linear combinations for monitoring vegetation. Remote Sens. Environ. 8, 127–150.
Ustin, S.L., Valko, P.G., Kefauver, S.C., Santos, M.J., Zimpfer, J.F., Smith, S.D., 2009. Remote sensing of biological soil crust under simulated climate change manipulations in the Mojave Desert. Remote Sens. Environ. 113, 317–328.
Vaughan, R.G., Hook, S.J., Calvin, W.M., Taranik, J.V., 2005. Surface mineral mapping at Steamboat Springs, Nevada, USA, with multi-wavelength thermal infrared images. Remote Sens. Environ. 99, 140–158.
Vaughan, R.G., Calvin, W.M., Taranik, J.V., 2003. SEBASS hyperspectral thermal infrared data: surface emissivity measurement and mineral mapping. Remote Sens. Environ. 85, 48–63.
Veste, M., Littmann, T., Breckle, S.-., Yair, A., 2001. The role of biological soil crusts on desert sand dunes in the northwestern Negev, Israel. In: Breckle, S., Veste, M., Wucherer, W. (Eds.), Sustainable Land Use in Deserts. Springer, Berlin, pp. 357–367.
Weber, B., Olehowski, C., Knerr, T., Hill, J., Deutschewitz, K., Wessels, D.C.J., Eitel, B., Büdel, B., 2008. A new approach for mapping of Biological Soil Crusts in semidesert areas with hyperspectral imagery. Remote Sens. Environ. 112, 2187–2201.
West, N.E., 1990. Structure and function of microphytic soil crusts in wildland ecosystems of arid to semi-arid regions. Adv. Ecol. Res. 20, 179–223.
Wu, N., Zhang, Y., Downing, A., 2009. Comparative study of nitrogenase activity in different types of biological soil crusts in the Gurbantunggut Desert, Northwestern China. J. Arid Environ. 73, 828–833.
Zaady, E., 1999. The role of microphytic soil crusts in desert ecosystems (in Hebrew). Ecol. Environ. 5, 70–76.
Zaady, E., Bouskila, A., 2002. Lizard burrows association with successional stages of biological soil crusts in an arid sandy region. J. Arid Environ. 50, 235–246.
Zaady, E., Karnieli, A., Shachak, M., 2007. Applying a field spectroscopy technique for assessing successional trends of biological soil crusts in a semi-arid environment. J. Arid Environ. 70, 463–477.
Zaady, E., Ben-David, E.A., Sher, Y., Tzirkin, R., Nejidat, A., 2010. Inferring biological soil crust successional stage using combined PLFA, DGGE, physical and biophysiological analyses. Soil Biol. Biochem. 42, 842–849.